Journal of Saudi Chemical Society (2016) **20**, 553–560

King Saud University

Journal of Saudi Chemical Society

www.ksu.edu.sa
www.sciencedirect.com

ORIGINAL ARTICLE

Physical properties of Fe doped Mn_3O_4 thin films synthesized by SILAR method and their antibacterial performance against *E. coli*

M.R. Belkhedkar [a,b], **A.U. Ubale** [a,*]

[a] *Nanostructured Thin Film Materials Laboratory, Department of Physics, Govt. Vidarbha Institute of Science and Humanities, VMV Road, Amravati 444604, Maharashtra, India*
[b] *Department of Physics, Shri Shivaji College, Akola 444003, Maharashtra, India*

Received 20 September 2014; revised 20 November 2014; accepted 24 November 2014
Available online 10 December 2014

KEYWORDS

Thin films;
Chemical synthesis;
Optical properties;
Electrical properties;
Antibacterial activity

Abstract Nanocrystalline Fe doped Mn_3O_4 thin films were deposited by successive ionic layer adsorption and reaction method onto glass substrates. The X-ray diffraction study revealed that Fe doped Mn_3O_4 films are nanocrystalline in nature. The morphological investigations were carried out by using field emission scanning electron and atomic force microscopy studies. The optical absorption measurements showed that Mn_3O_4 films exhibit direct band gap energy of the order of 2.78 eV and it increased to 2.89 eV as the percentage of Fe doping in it increases from 0 to 8 wt.%. The room temperature electrical resistivity of Mn_3O_4 increases from 1.84×10^3 to 2.64×10^4 Ω cm as Fe doping increases from 0 to 8 wt.%. The SILAR grown Mn_3O_4 showed antibacterial performance against *Escherichia coli* bacteria which improved remarkably with doping.

1. Introduction

For the last twenty years, nanocrystalline thin films of transition-metal oxides have been extensively studied owing to their fascinating novel physical and chemical properties. The fabrication of nanocrystalline thin films in unlimited quantities with outstanding fundamental and potential technological consequences is the crucial challenge of modern materials research. At nano size, semiconductor crystallite due to quantum confinement of the electronic states shows different physical and chemical properties in comparison with bulk crystals. These ultra-thin semiconductor thin films have potential applications in various types of optoelectronic devices. Several efforts have been made by researchers to synthesize thin metal oxide semiconductor thin films by a simple and economic chemical method [1–5]. In the present work an attempt was made to deposit nanocrystalline Fe doped Mn_3O_4 thin films by the simple chemical successive ionic layer adsorption and reaction method. It is well known that manganese oxide has different phases such as MnO, MnO_2, Mn_2O_3, and Mn_3O_4

* Corresponding author at: Nanostructured Thin Film Materials Laboratory, Department of Physics, Govt. V.I.S.H., Amravati 444604, Maharashtra, India. Tel.: +91 721 2531706; fax: +91 721 2531705.
E-mail address: ashokuu@yahoo.com (A.U. Ubale).
Peer review under responsibility of King Saud University.

Production and hosting by Elsevier

http://dx.doi.org/10.1016/j.jscs.2014.11.004

depending on oxidation states of Mn. Among them Mn_3O_4 is a promising material which is useful in various types of applications such as catalysts [6], rechargeable lithium batteries [7], electrochemical materials [8], electrochemical sensors [9], supercapacitors [10] etc. In addition, this utmost stable oxide phase of manganese has been used as an absorbing material in various types of optoelectronic devices [11]. As per the literature many researchers have prepared manganese oxide thin films by doping suitable metal ions to modify their structural, morphological, optical and electrical properties. Bayon et al. [12] have studied the optical properties of dip coated copper doped manganese oxide thin films. Hussain et al. [13] have investigated structural and electrical properties of lithium doped manganese oxide thin films grown by pulsed laser deposition. However, Singh et al. [14] have reported microstructural and electrochemical properties of lithium doped manganese oxide thin films grown by pulsed laser deposition. Dakhel [15] has reported dc conduction mechanisms in dysprosium doped manganese oxide thin films grown on Si substrates by the thermal deposition method. Yang [16] has studied supercapacitor application of pulsed laser deposited cobalt-doped manganese oxide thin films. Moon et al. [17] have synthesized Li doped manganese oxide thin films by R.F. magnetron sputtering and investigated the effect of film stress on its microstructure, surface morphology, and electrochemical characteristics. However, as per our knowledge no report is available on structural and electrical properties of Fe doped Mn_3O_4 thin films grown by the simple and economic chemical method.

In the present work, the simple and economic chemical method, successive ionic layer adsorption and reaction method has been successfully employed to deposit Fe doped Mn_3O_4 thin films at room temperature. The structural, morphological, optical and electrical characterizations of Fe doped Mn_3O_4 thin films were investigated. In addition, the antibacterial performance of the films against *Escherichia coli* bacteria is discussed.

2. Experimental

2.1. Preparation Fe doped Mn_3O_4 thin films

In the SILAR method, to deposit nanocrystalline thin films, substrate is alternately immersed into cationic and anionic precursors repeatedly. After each immersion, the substrate is rinsed in deionized water to remove loosely bound species from it. To deposit Fe doped Mn_3O_4 thin films, 0.06 M $FeCl_3$ of pH <1 and 0.3 M $MnCl_2$ of pH 12 were used as cationic precursors along with dilute NaOH (pH $\approx$ 12) solution as an anionic precursor. Several trials were carried out to optimize the various deposition parameters for α-Fe_2O_3 and Mn_3O_4 thin films separately. The optimized deposition parameters for Mn_3O_4 films were already explained elsewhere [18]. To deposit α-Fe_2O_3 thin films, a well cleaned glass substrate was immersed in cationic precursor for 20 s where Fe^{3+}. Ions were adsorbed on the substrate surface. The substrate was then rinsed in deionized water for 20 s to remove loosely bound ions. Finally, it was immersed in NaOH solution for 20 s, where OH^- ions react with Fe^{3+} ions to form α-Fe_2O_3 species. This was followed by rinsing in deionized water for 20 s to remove loose α-Fe_2O_3 species from the substrate surface. This completes one SILAR deposition cycle for α-Fe_2O_3. Several deposition trials were performed by varying the concentration of Fe source to match the growth rate of α-Fe_2O_3 film formation with Mn_3O_4. It was observed that the growth rate of Mn_3O_4 and α-Fe_2O_3 at 0.06 and 0.3 M concentration of $FeCl_3$ and $MnCl_2$ was approximately same. Hence, for the present work, to deposit Fe doped Mn_3O_4 thin films 0.06 and 0.3 M concentrations of $FeCl_3$ and $MnCl_2$ were considered. To achieve 0, 2, 4, 6 and 8 wt.% doping of Fe in Mn_3O_4 the SILAR deposition cycles for Fe_2O_3: Mn_3O_4 composition were taken as (0:50), (1:49), (2:48), (3:47) and (4:46) respectively.

2.2. Characterization techniques

In the present work, thickness of the film was measured by the gravimetric weight difference method using relation,

$$t = \frac{m}{\rho \times A} \tag{1}$$

.where 'm' is the mass of the deposited film measured by sensitive microbalance; 'A' is the area of the deposited film and 'ρ' is the density of the deposited materials in bulk form. The crystal structure of the deposited film was identified by grazing incidence X-ray diffraction Xpert PRO PANalytical diffractometer. The film surface morphology was observed by using field emission scanning electron microscope (Model: SUPRA 40) and atomic force microscope (Model: Nanonics Multiview 2000™, Israel). The optical absorption studies were carried out in the wavelength range 350–750 nm using ELICO ® Double Beam SL 210 UV–VIS spectrophotometer. The variation of electrical resistivity with temperature was measured using the dc two point probe technique with a digital electrometer and stabilized power supply.

2.3. Antibacterial test

The antibacterial performance of Fe doped Mn_3O_4 thin films against *E. coli* was investigated using the spread plate technique. Initially, the culture of *E. coli* bacteria was prepared in nutrient broth. The loopful culture of *E. coli* organisms was then inoculated into 20 mL sterilized nutrient broth and incubated at 310 K temperature for 24 h to obtain well grown bacteria. Then, 20 µL culture of *E. coli* was inoculated on Fe doped Mn_3O_4 deposited and undeposited glass substrates of area 1 cm^2 with the help of inoculating needle. These glass slides were then placed in previously sterilized petri dishes and incubated at 310 K for 24 h. After the successful incubation these slides were then washed by ultrasonication using 3 mL buffer peptone solution to detach bacteria from the substrate. Further, 20 µL washed buffer peptone solution was then inoculated on nutrient agar plates by the spread plate technique and incubated at 310 K for 24 h to obtain viable bacteria. After successful incubation the viable bacterial colonies were counted and antibacterial efficiency was calculated using the relation [19],

$$r = \frac{(N_0 - N)}{N_0} \times 100\% \tag{2}$$

where, 'r' is the antibacterial efficiency, 'N_0' is the number of viable bacteria with undeposited (standard) sample in the petri dish and 'N' is the number of viable bacteria with deposited sample in the petri dish.

3. Results and discussion

3.1. Film formation mechanism

The SILAR deposition mechanism involves the ion-by-ion deposition at nucleation sites on the substrate surfaces. It is well known that, in aqueous solution $MnCl_2$, $FeCl_3$ and NaOH dissociates as,

$$MnCl_2 \leftrightarrow Mn^{2+} + 2Cl^- \quad (3)$$

$$FeCl_3 \leftrightarrow Fe^{3+} + 3Cl^- \quad (4)$$

$$NaOH \leftrightarrow Na^+ + OH^- \quad (5)$$

Initially, the substrate was immersed in $MnCl_2$ precursor, where Mn^{2+} ions get adsorbed on the substrate. After rinsing in deionized water, the substrate was immersed in an alkaline medium i.e. in NaOH precursor, where $2OH^-$ is from the solution reacts with Mn^{2+} on the substrate surface to give $Mn(OH)_2$,

$$Mn^{2+} + 2OH^- \rightarrow n(OH)_2 \quad (6)$$

To remove loose species of $Mn(OH)_2$, the substrate was removed from NaOH precursor and immersed in rinsing water. During this process $Mn(OH)_2$ was transformed to Mn_3O_4 by oxidation with atmospheric oxygen [18],

$$6Mn(OH)_2 + O_2 \rightarrow 2Mn_3O_4 + 6H_2O \quad (7)$$

Finally, the Mn_3O_4 coated glass substrate was immersed in $FeCl_3$ precursor, where Fe^{3+} ions get adsorbed on the substrate to give $Fe^{3+}Mn_3O_4$

$$Mn_3O_4 + FeCl_3 \rightarrow Fe^{3+}Mn_3O_4 \quad (8)$$

Further, when the substrate was immersed in NaOH precursor solution, adsorption of hydroxide ions on the substrate takes place as,

$$Fe^{3+}Mn_3O_4 + 3OH^- \rightarrow Fe(OH)_3Mn_3O_4 \quad (9)$$

After annealing the film in air atmosphere at 573 K composite α-Fe_2O_3: Mn_3O_4 material is formed as,

$$2Fe(OH)_3Mn_3O_4 \frac{573K}{3h} \rightarrow 2\alpha - Fe_2O_3 : Mn_3O_4 \quad (10)$$

3.2. Structural studies

Fig. 1 shows GIXRD patterns of Fe doped manganese oxide thin films deposited onto glass substrates by the SILAR method. The (1 1 1), (1 1 2), (1 3 4), (2 0 0) and (1 5 3) peaks observed in the X-ray diffraction patterns corresponds to the orthogonal structure of Mn_3O_4 [JCPDS 75-0765]. However (0 1 2), (1 1 3) and (0 2 4) peaks correspond to the rhombohedral structure of α-Fe_2O_3 [JCDPS 79-0007]. It is observed that the intensity of the diffraction peaks is decreased with the percentage of Fe doping in Mn_3O_4 films. The average crystallite size of the film was determined by using the Scherrer formula [20],

$$D = \frac{0.9\lambda}{\beta \, Cos\theta} \quad (11)$$

where 'λ' is the wavelength used (0.154 nm); 'β' is the angular line width at half maximum intensity in radians; 'θ' is the Bragg's angle. It is seen that the average crystallite size of the as deposited Mn_3O_4 is 43 nm and it decreases to 29 nm as Fe doping increases to 8 wt.%. (Table 1)

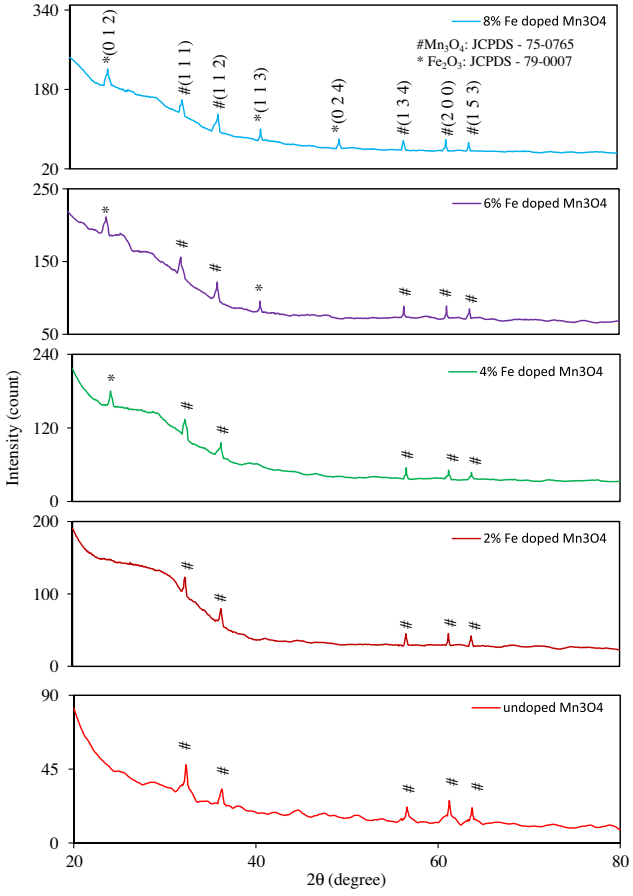

Figure 1 GIXRD patterns of Fe doped Mn_3O_4 thin films.

Table 1 Crystallite size of Fe doped Mn_3O_4 thin films with doping percentage.

Wt.% of Fe in Mn_3O_4	Film thickness (nm)	Average crystallite size from	
		GIXRD (nm)	FESEM (nm)
0	104.6	43	46
2	105	38	41
4	106	32	35
6	108	30	32
8	107	29	30

3.3. Surface morphology

The surface morphology of the Fe doped manganese oxide thin films deposited onto glass substrates by the SILAR method by changing Fe doping from 0 to 8 wt.% was examined using FESEM images (Fig. 2). The images showed uniform distribution of spherical nanograins of Mn_3O_4 and α-Fe_2O_3 over the entire substrate surface. The size of the nanograins varies between 27 to 49 nm depending on the doping percentage and it agrees well with XRD results (Table 1). Also

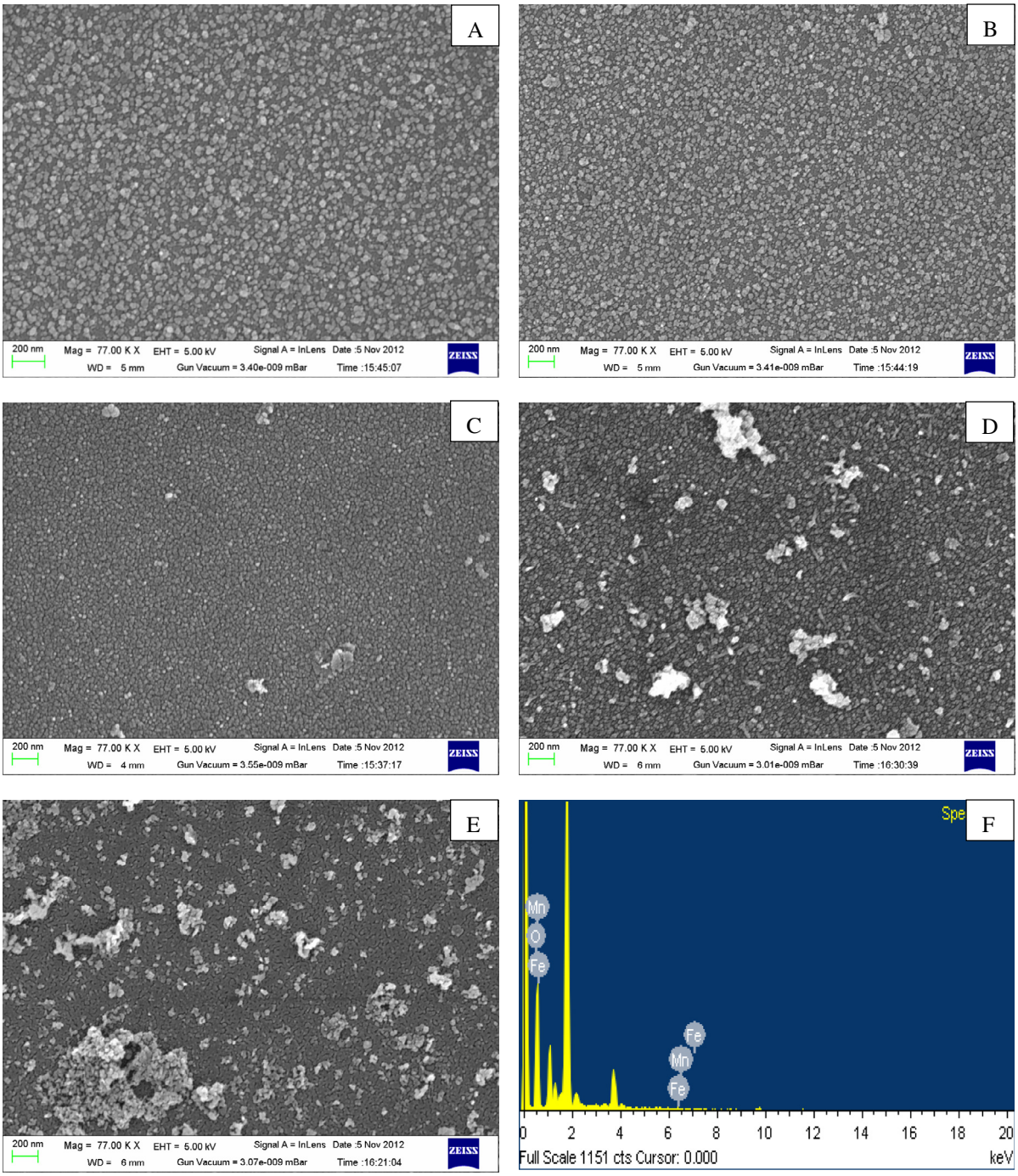

Figure 2 FESEM images of Fe doped Mn_3O_4 thin films with Fe doping percentage: (A) 0 wt.%, (B) 2 wt.%, (C) 4 wt.%, (D) 6 wt.% and (E) 8 wt.%, and (F) typical EDX spectrum of 2 wt.% Fe doped Mn_3O_4 thin film.

as the doping percentage of Fe increases above 4 wt.% the agglomeration of nanograins is observed in terms of overgrowth on the background of the homogeneous granular structure. A typical EDX spectrum shown in Fig. 2(F) confirms doping of Fe element in the Mn_3O_4 film material. However, the other peaks in the EDX pattern are due to the glass substrate.

The surface morphology of Fe doped Mn_3O_4 films were further investigated by using atomic force microscope in tapped mode. Fig. 3 shows 3D AFM images of Fe doped Mn_3O_4 thin films. The films are uniform, homogeneous and well covered to the glass substrates. The rms roughness of Mn_3O_4 film decreases as Fe doping in it increases from 0–4 wt.% owing to its improved nanocrystalline nature. Above 4 wt.% doping of Fe rms roughness of the films increases due to overgrowth as seen in FESEM images. The other morphological parameters estimated from AFM analysis are tabulated in Table 2. The average height estimated is also in good agreement with films thickness estimated using the gravimetric method.

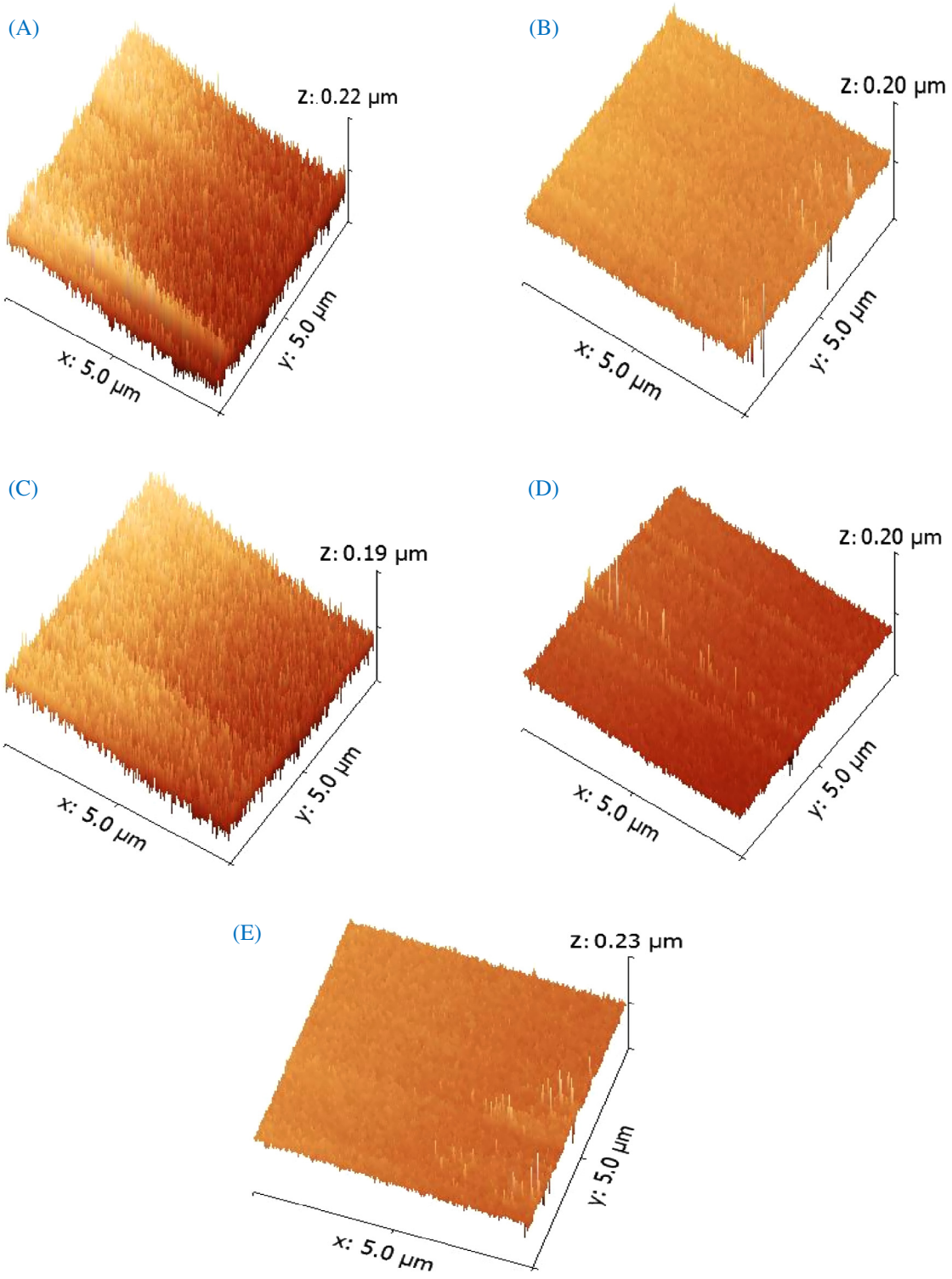

Figure 3 3D AFM images of Fe doped Mn_3O_4 thin films with doping percentage (A) 0 wt.%, (B) 2 wt.%, (C) 4 wt.%, (D) 6 wt.% and (E) 8 wt.%.

3.4. Optical studies

The optical properties of undoped and Fe doped Mn_3O_4 thin films deposited onto glass substrates were studied in the wavelength range 350–750 nm at room temperature (Fig. 4). It was observed that the optical absorption of Mn_3O_4 decreases as doping percentage of Fe increases. The optical absorption coefficient 'α' for Mn_3O_4 at 350 nm wavelength is of the order of 0.1805 cm^{-1} and it decreases to 0.0516 cm^{-1} as the doping of Fe rises to 8 wt.%, indicating that Fe doping increases the

Table 2 Morphological parameters of Fe doped and undoped Mn_3O_4 thin films.

Fe doping in Mn_3O_4 (wt.%)	RMS roughness Rq (nm)	Average surface roughness Ra(nm)	Maximum height (nm)	Average height (nm)	Grain orientation (pi)
0	42.67	34.38	226.1	110.73	0.07
2	44.13	33.19	209.2	113.93	0.17
4	32.21	24.89	195.5	107.61	0.07
6	37.83	31.75	202.6	110.05	0.19
8	44.56	35.87	236.1	115.63	0.20

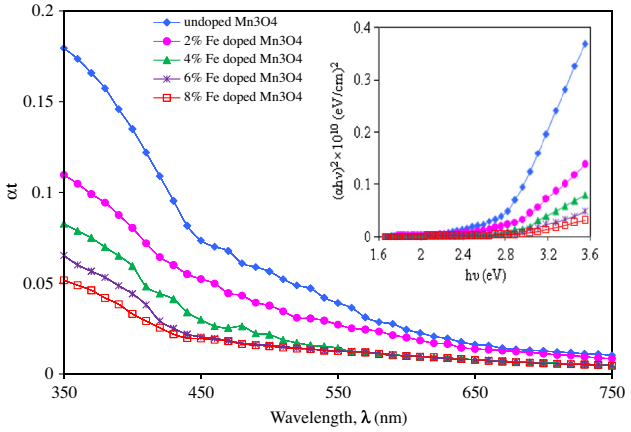

Figure 4 Plots of optical absorption against wavelength (λ) (Inset shows the plots of $(\alpha h\upsilon)^2$ versus $h\upsilon$) for Fe doped Mn_3O_4 thin films.

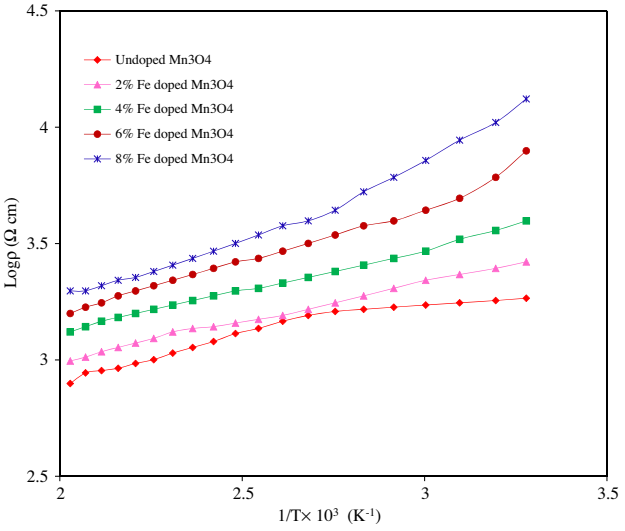

Figure 5 Plots of $\log\rho$ versus $10^3/T$ for Fe doped Mn_3O_4 thin films.

transparency of the film. The optical band gap energy (Eg) of undoped and Fe doped Mn_3O_4 films is calculated using the equation [21],

$$\alpha h\upsilon = A(h\upsilon - Eg)^n \tag{12}$$

where, 'α' is absorption coefficient, 'Eg' is band gap, 'A' is a constant and 'n' is equal to 1/2 for direct and 2 for indirect transition. The plots of $(\alpha h\upsilon)^2$ versus $h\upsilon$ for Fe doped Mn_3O_4 thin films are shown in the inset of Fig. 4. The optical band gap energy of Mn_3O_4 film is 2.78 eV and it increases to 2.89 eV as Fe doping increases from 0 to 8 wt.% (Table 3). This increase in the direct band gap energy of Mn_3O_4 films with Fe doping is attributed to Moss-Burstein effect. When the concentration of Fe doping in the Mn_3O_4 increases, the conduction band becomes significantly filled and the lowest energy states in the conduction band are blocked, as a results the absorption interband moves to higher energy states and blue shift occurs [22].

3.5. Electrical resistivity

The variation of electrical resistivity of Fe doped Mn_3O_4 thin films with temperature was studied using a dc two point probe method. Fig. 5 shows the variation of log (ρ) with the reciprocal of the temperature. The electrical resistivity of films decreases with an increase in temperature that confirms their semiconducting nature. The electrical resistivity of the Mn_3O_4 film at 333 K temperature is of the order of $1.84 \times 10^3\ \Omega$ cm and it increases to $2.6 \times 10^4\ \Omega$ cm as the Fe doping increases to 8 wt.%. This increased electrical resistivity

Table 3 Variation of optical band gap and antibacterial efficiency of Mn_3O_4 films with Fe doping.

Fe doping in Mn_3O_4 (wt.%)	Optical band gap energy (eV)	Activation energy (eV)	Antibacterial efficiency (%)
0	2.78	0.12	86
2	2.80	0.13	87
4	2.82	0.14	88
6	2.85	0.19	89
8	2.89	0.29	90

is attributed to the reduced crystallite size of the film with Fe doping percentage. As the grain size of the deposited film decreases, the charge carrier density of the film decreases, as a result film resistivity increases. On the other hand, in the Fe doped Mn_3O_4 film, Fe-ions act as acceptors and majority charge carrier Mn-ions act as donors. As the Fe content in Mn_3O_4 thin films increases, the mobility and concentration of Mn-ions decrease that increases its electrical resistivity [23]. The activation energies of Fe doped Mn_3O_4 films are calculated using the relation,

$$\rho = \rho_o\left(\frac{E_a}{KT}\right) \tag{13}$$

where 'ρ' is the resistivity at temperature T, 'ρ_0' is a constant; 'K' is the Boltzmann constant and 'E_a' is the activation energy.

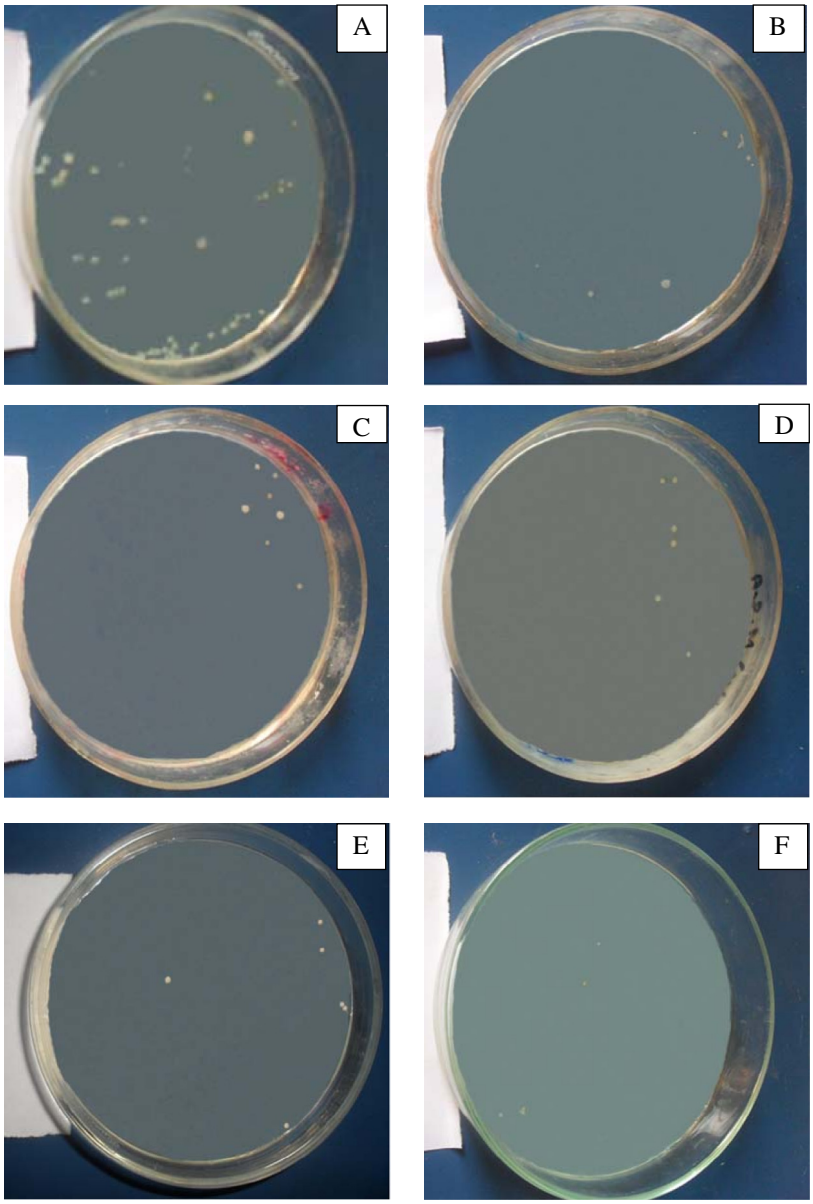

Figure 6 Test results on *E. coli* after 24 h: incubated with (A) undeposited glass substrate, and Fe doped Mn_3O_4 thin films: (B) 0 wt.%, (C) 2 wt.%, (D) 4 wt.%, (E) 6 wt.% and (F) 8 wt.%.

The activation energy of Fe doped Mn_3O_4 thin film deposited onto glass substrate is increased from 0.12 to 0.29 eV depending on doping percentage (Table 3). This increase in activation energy is attributed to the improved nanocrystalline nature of the film.

3.6. Antibacterial activity

The antibacterial efficiency of the Fe doped Mn_3O_4 thin films against *E. coli* bacteria was studied. The test results of *E. coli* bacteria incubated for 24 h on undeposited glass substrate and Fe doped Mn_3O_4 thin film surfaces are shown in Fig. 6. It was observed that, the antibacterial efficiency of un-doped Mn_3O_4 film is 86% and it increases to 91% as doping of Fe increases from 0 to 8 wt.% (Table 3). This increased antibacterial efficiency with doping is attributed to the increased contribution of Mn, Fe and hydroxyl ions released from the surface that kills *E. coli* microorganisms. Also with Fe doping, the film becomes more nanocrystalline and hence provides more surface area for antibacterial activity.

4. Conclusions

Nanocrystalline Fe doped Mn_3O_4 thin films were successfully grown by the successive ionic layer adsorption and reaction method onto glass substrates. The GIXRD, FESEM and AFM analysis confirm that SILAR grown films are nanocrystalline in nature. The optical band gap energy, electrical resistivity and activation energy of Mn_3O_4 thin films increases with Fe doping owing to improved nanocrystalline nature. The morphological study showed that the nanocrystalline nature of the film increases with doping. The antibacterial efficiency of Mn_3O_4 film against *E. coli* bacteria increases with Fe doping.

References

[1] G. Hodes, Isr. J. Chem. 33 (1993) 95.
[2] A. Hagfeldt, M. Gratzel, Chem. Rev. 95 (1995) 49.
[3] S. Hotchandani, P.V. Kamat, J. Electrochem. 139 (1992) 1630.
[4] A.U. Ubale, V.P. Deshpande, J. Alloys Compd. 500 (2010) 138.
[5] J.J. Hassan, M.A. Mahdi, A. Ramizy, H. Abu Hassan, Z. Hassan, Superlattices Microstruct. 53 (2013) 31.
[6] J. Zhang, J. Du, H. Wang, J. Wang, Z. Qu, L. Jia, Mater. Lett. 65 (2011) 2565.
[7] E. Machefaux, A. Verbaere, D. Guyomard, J. Power Sources 157 (2006) 443.
[8] S. Xing, Z. Zhou, Z. Ma, Y. Wu, Mater. Lett. 65 (2011) 517.
[9] W.B.S. Machini et al, Sens. Actuators, B 181 (2013) 674.
[10] Q. Huang, X. Wang, J. Li, Electrochim. Acta 52 (2006) 1758.
[11] D.P. Dubal, D.S. Dhawale, R.R. Salunkhe, V.J. Fulari, C.D. Lokhande, J. Alloys Compd. 497 (2010) 166.
[12] R. Bayon, G.S. Vicente, C. Maffiotte, A. Morales, Sol. Energy Mater. Sol. Cells 92 (2008) 1211.
[13] O.M. Hussain, K.H. Krishna, V.K. Vani, C.M. Julien, Ionics 13 (2007) 455.
[14] D. Singh, W.S. Kim, V. Craciun, H. Hofmann, R.K. Singh, App. Surf. Sci. 197–198 (2002) 516.
[15] A.A. Dakhel, Microelectron. Reliab. 46 (2006) 1303.
[16] D. Yang, J. Power Sources 198 (2012) 416.
[17] H.S. Moon, W.H. Lee, P.J. Reucroft, J.W. Park, J. Power Sources 119–21 (2003) 710.
[18] A.U. Ubale, M.R. Belkhedkar, Y.S. Sakhare, A. Singh, C. Gurada, D.C. Kothari, Mater. Chem. Phys. 136 (2012) 1067.
[19] W. Zhang, Y. Chen, S. Yu, S. Chen, Y. Yin, Thin Solid Films 516 (2008) 4690.
[20] A.U. Ubale, Y.S. Sakhare, M.V. Bhute, M.R. Belkhedkar, A. Singh, Solid State Sci. 16 (2013) 134.
[21] M.A. Mahdi, J.J. Hassan, Z. Hassan, S.S.J. Ng, J. Alloys Compd. 541 (227–23) (2012) 3.
[22] A.A. Ziabari, S.M. Rozati, Phys. B 407 (2012) 4512.
[23] T. Miyata, H. Tanaka, H. Sato, T. Minami, J. Mater. Sci. 41 (2006) 5531.